THEF-NIJM 24.04
arXiv:2408.03812

Nucleon-quark mixed matter and neutron star EOS

Y. Yamamoto[1], N. Yasutake[2], and Th.A. Rijken[3,1]

[1]*RIKEN Nishina Center, 2-1 Hirosawa, Wako, Saitama 351-0198, Japan*
[2]*Department of Physics, Chiba Institute of Technology,*
2-1-1 Shibazono Narashino, Chiba 275-0023, Japan
[3]*IMAPP, Radboud University, Nijmegen, The Netherlands*

Abstract

The nucleon-quark mixed matter is defined in the Brueckner-Hartree-Fock framework, in which quark densities are determined by equilibrium conditions between nucleon and quark chemical potentials, and nucleon-quark interactions play critical roles for resulting EoSs (equation of state). The two models of EoSs are derived from the nucleon-quark mixed matter (NQMM): The NQMM-A EoSs are based on the simple assumption that nucleons and free quarks occupy their respective Fermi levels and their Fermi spheres overlap from each other. In NQMM-B EoSs, the quark Fermi repulsion effect is incorporated on the basis of quakyonic matter, meaning that the nucleon Fermi levels are pushed up from the quark Fermi sphere by the Pauli exclusion principle. For the NQMM-A EoSs, the neutron-star mass-radius (MR) curves are pushed up above the region of $M \sim 2.1 M_\odot$ and $R_{2.1M_\odot} \sim 12.5$ km indicated by the recent observations, as the qN repulsions increase. For the NQMM-B EoSs, the similar results are obtained by the combined contributions from the qN repulsion and the quark Fermi repulsion. In both models of EoSs, the important roles of the qN di-quark exchange repulsions are demonstrated to reproduce reasonable values of M_{max} and $R_{2.1M_\odot}$.

I. INTRODUCTION

The massive neutron stars (NS) with masses over $2M_\odot$ have been reliably established by the observations of J1614−2230 [1], J0348+0432 [2], J0740+6620 [3] and J0952-0607 [4]. Despite these observations of massive neutron stars over $2M_\odot$, the hyperon mixing in neutron-star matter brings about a remarkable softening of the EoS (equation of state) and a maximum mass is reduced to a value far less than $2M_\odot$, being called "hyperon puzzle in neutron stars". The EoS softening is caused by changing of high-momentum neutrons at Fermi surfaces to low-momentum hyperons via strangeness non-conserving weak interactions overcoming rest masses of hyperons. Generally, such mechanisms can be due to possible appearance of other hadronic degrees of freedom, such as Δ isobars [5], meson condensates [6–10] or quark phases [11–22]. Since such mechanisms of EoS softening are inevitable in neutron-star matter, it has been one of the central issues in this field to model EoSs giving star masses over $2M_\odot$.

From the analyses for the X-ray data taken by the *Neutron Star Interior Composition Explorer* (NICER) and the X-ray Multi-Mirror (XMM-Newton) observatory, the radius information of NSs have been obtained for the massive NS PSR J0740+6620 [23–27]. The radius information of massive NSs give important constraints for neutron-star EoSs, which are demonstrated critically by reproducing the neutron-star radii [22].

Recently, they have given a more precise measurement of the radius of PSR J0740+6620 using updated NICER data as $R = 12.49^{+1.28}_{-0.88}$ km with the determined mass $M = 2.08 \pm 0.07 M_\odot$ [26]. We adopt their median values of $M = 2.1M_\odot$ and the radius $R_{2.1M_\odot} = 12.5$ km at $M = 2.1M_\odot$ for comparison with our calculated results. These values are used as the criterion for EoSs, which is far more severe than the one using only the mass values such as $2M_\odot$. In mass and radius (MR) relations of neutron stars, the criterion for MR curves is to reach the point ($M = 2.1M_\odot$, $R_{2.1M_\odot} =$ 12.5 km).

There have been proposed several mechanisms to reproduce masses over $2M_\odot$, solving the "hyperon puzzle". Among them, the baryonic approach is to introduce the repulsive hyperonic three-body forces at the baryon level [28–35]. In [30–32], the multi-pomeron exchange potential (MPP) was introduced as a model of universal repulsions among three and four baryons on the basis of the extended soft core (ESC) baryon-baryon interaction model developed by two of the authors (T.R. and Y.Y.) and M.M. Nagels [36–38]. In their modeling for hyperonic three-body repulsions, the EoS softening by hyperon mixing is not completely recovered by the MPP repulsions: The maximum masses do not significantly exceed $2M_\odot$, even if MPP repulsions are taken strong enough. It seems difficult to reproduce both of $M_{max} \sim 2.1M_\odot$ and $R_{2.1M_\odot} \sim 12.5$ km by hadronic-matter EoSs with hyperon mixing, as discussed in the following section.

The challenging subject is to study quark deconfinement phase transitions from a hadronic-matter EoS to a sufficiently stiff quark-matter EoS giving $M_{max} \sim 2.1M_\odot$ and $R_{2.1M_\odot} \sim 12.5$ km. It is known that quark-hadron phase transitions should be crossover or at most of weak first-order in order to obtain EoSs stiff enough, because strong first-order transitions soften EoSs remarkably [11–21]. Then, it is essential that repulsive effects in quark phases are needed to result in massive stars over $2M_\odot$. Without such repulsive effects, the quark mixing in neutron-star matter brings about a remarkable softening of the EoS and a maximum mass is reduced to a value far less than $2M_\odot$, where the softening is caused by changing of high-momentum neutrons to low-momentum

quarks. In the Nambu-Jona-Lasinio (NJL) model, for instance, repulsions to stiffen EoSs are given by vector interactions. In the case of our quark-hadron transition (QHT) model [21, 22], the quark-quark (qq) repulsions composed of meson-exchange and one-gluon-exchange potentials.

Another type of quark phase in neutron-star interiors is given by the so-called quarkyonic matter [22, 39–46], where the degrees of freedom inside the Fermi sea are treated as free quarks, and nucleons exist at the surface of the Fermi sea. In the quarkyonic matter, the existence of free quarks inside the Fermi sphere gives nucleons extra kinetic energy by pushing them up to higher momenta, leading to increasing pressure. This mechanisms stiffening EoSs are completely different from the quark-hadron transition models in which the essential roles for EoS stiffening are played by the qq repulsions. In our previous work [22], we investigated the roles of quark-quark (qq) and quark-neutron (qn) interactions in the quakyonic matter, which were not taken into account in [41]. However, there remain two important problems in our treatment: The first is that the roughly approximated version is used for the qn interactions. The second is that in quakyonic matter formalism [41] the thickness parameter Δ for the neutron Fermi layer plays the decisive role for neutron-star MR (mass-radius) curves, and then no important conclusions can be drawn regarding minor effects of qn/qq interactions.

In this paper, we propose the nucleon-quark mixed matter (NQMM) model in the Brueckner-Hartree-Fock (BHF) framework, which is suitable to clarify effects of quark-nucleon (qN) and qq interactions. As a first step, in treating mixed-matter hyperon and s-quark mixings are not included for simplicity.

In this framework quark densities in nucleon-quark mixed matter are determined by equilibrium conditions between chemical potentials of neutrons and free u and d quarks without using ad hoc parameters such as the Fermi-layer thickness Δ. We define here the two models of nucleon-quark mixed matter; NQMM-A and NQMM-B. In NQMM-A, nucleons (free quarks) occupies simply their Fermi sphere from zero momentum to Fermi momentum k_F^N (k_F^q). In NQMM-B, the Fermi repulsion effects for nucleons are incorporated on the basis of quakyonic matter, in which nucleon Fermi levels are pushed up to those with higher momenta by the Fermi exclusion for nucleons from the quark Fermi sphere. In the derivations of EoSs for NQMM-A and NQMM-B, calculations are performed with use of the realistic qN interactions given in [49, 50] together with the realistic NN and qq interactions. The derived EoSs are used to obtain the neutron-star MR curves by solving the Tolmann-Oppenheimer-Volkoff (TOV) equations. Then, it is possible to study how the conditions of reproducing $M_{max} \sim 2.1 M_\odot$ and $R_{2.1M_\odot} \sim 12.5$ km are realized by our EoSs.

This paper is organized as follows: In Sect.II-A, the hadronic-matter EoSs in our previous works [30–32] are recapitulated, which is the basis of deriving the nucleon-quark mixed matter EoS. In Sect.II-B, our qN interactions are explained, which play important roles for the derived EoSs and neutron-star MR curves. In Sect.II-C, our EoSs for NQMM-A and NQMM-B are formulated in the BHF framework. In Sect.III-A, the calculated results are shown for densities, energy densities, chemical potentials and pressures in nucleon-quark mixed matter, leading to our EoSs. In III-B, the MR curves of neutron stars are obtained by solving the TOV equation with our EoSs for NQMM-A and NQMM-B. The conclusion of this paper is given in Sect.IV.

II. NUCLEON-QUARK MIXED MATTER

A. Toward quark mixing in hadronic matter

The hadronic matter is defined as β-stable hyperonic nuclear matter. As a starting point for investigating the nucleon-quark mixed matter, we recapitulate a typical hadronic-matter EoS composed of n, p^+, Λ, e^- in the BHF framework with use of the ESC baryon-baryon (BB) interaction model [30–32].

Our baryonic interactions are composed of two-body part V_{BB} and three-body part V_{BBB}. BB G-matrix interactions $\mathcal{G}_{BB}$ are derived from BB bare interactions V_{BB} or $V_{BB}+V_{BBB}$ [30]. They are given for each (BB', T, S, P) state, T, S and P being isospin, spin and parity in a two-body state, respectively, and represented as $\mathcal{G}^{TSP}_{BB'}$. In the following sections, we need only the nucleon-nucleon sectors, $\mathcal{G}^{SP}_{NN}$.

As is well known, the nuclear-matter EoS is stiff enough to assure neutron-star masses over $2M_\odot$, if the strong three-nucleon repulsion is taken into account. However, there appears a remarkable softening of EoS by inclusion of exotic degrees of freedom such as hyperon mixing. As one of the ideas to avoid this "hyperon puzzle", it was proposed that the three-body repulsions worked universally for every kind of baryons [28]. In [30–32], the multi-pomeron exchange potential (MPP) was introduced as a model of universal repulsions among three and four baryons. The recent ESC works are mentioned in [36–38].

In [32] they proposed three versions of MPP (MPa, MPa$^+$, MPb), where MPa and MPa$^+$ (MPb) include the three- and four-body (only three-body) repulsions. The obtained MR curves are given in Fig.3 [32], where the curves move upwards with increase of MPP repulsions. The important criterion in this paper is the value of $R_{1.4M_\odot}$: We adopt MPb, giving $R_{1.4M_\odot} \approx 12.4$ km. As shown later, this $R_{1.4M_\odot}$ value of MPb persists in the nucleon-quark mixed matter EoS.

In [32], values of M_{max} and $R_{2M\odot}$ are obtained from the EoSs including MPb for β-stable nuclear matter with and without Λ mixing, which are $M_{max}/M_\odot = 2.06$ (2.19), and $R_{2M_\odot} = 11.3$ km (11.8 km) for the EoS with (without) Λ mixing. The values of $R_{2M_\odot}$ for the hadronic matter EoSs are substantially smaller than 12.5 km. By such hadronic-matter EoSs, it difficult to satisfy the criterion reproducing ($M_{max} = 2.1M_\odot$, $R_{2.1M_\odot} = 12.5$ km). It is commented that the three-nucleon repulsion included in MPb is stronger than the corresponding one (UIX) in the standard model by APR [47] giving rise to $R_{1.4M_\odot} \approx 11.6$ km [48].

In order to explore possibilities of getting larger values of $R_{2.1M_\odot}$ under $M_{max} \sim 2.1M_\odot$, the BHF framework for hadronic matter is extended to the nucleon-quark mixed matter composed of n, p, u, d and e^-, where strangeness degrees of freedom are not taken into account for simplicity. Because u and d quarks are treated in the BHF base, it is necessary to use quark-nucleon (qN) and quark-quark (qq) two-body interactions in BHF calculations as well as NN interactions. In the treatment of quark mixing, we learn from the simple case of Λ mixing in neutron matter where Λ mixing rates are determined by chemical equilibrium conditions $\mu_n = \mu_\Lambda$ with chemical potentials μ_n and μ_Λ of neutron and Λ, respectively. In the case of neutron-quark mixing, correspondingly, quark mixing rates in neutron matter are determined by chemical equilibrium conditions $\mu_n = \mu_u + 2\mu_d$ with chemical potentials μ_u and μ_d of u and d quarks, respectively.

B. qN and qq interactions

In BHF calculations of nucleon-quark mixed matter, quark-quark (qq) and quark-nucleon (qN) two-body interactions are needed as well as NN interactions. In our previous works [21, 22], the quark-matter calculations were performed with use of the two-body qq interaction. The basic part of this qq interaction is given by the extended meson-exchange (EME) potential $V_{EME}^{(qq)}$, derived from the ESC BB potential so that the qqM couplings are related to the BBM couplings through folding procedures with Gaussian baryonic quark wave functions. In [21], this qq potential was named as Q0, and the more repulsive versions are given by adding instanton-exchange and one-gluon exchange (OGE) potentials (Q1), and furthermore the multi-pomeron exchange potential (Q2). In this work, we use the simplified version Q3 composed of EME and OGE potentials, being adjusted so as to be similar to Q2. Qualitatively, however, resulting EoSs do not much depend on whether Q0, Q1, Q2 or Q3 is used for qq interactions, because quark densities in nucleon-quark mixed matter are not large compared to nucleon densities and partial pressures of free quarks are far smaller than those of nucleons.

In [49], qq potentials $V_{EME}^{(qq)}$ and qN potentials $V_{EME}^{(qN)}$ are derived together, in which meson-quark-quark and meson-nucleon-nucleon couplings are determined consistently. In addition to the meson-exchange potentials, we introduce the di-quark exchange (DQE) potential $V_{DQE}^{(qN)}$ derived in [50]: The total qN interaction is

$$V^{(qN)} \;=\; V_{EME}^{(qN)} + V_{DQE}^{(qN)} \,. \tag{2.1}$$

As shown later, $V_{DQE}^{(qN)}$ plays a more important role than $V_{EME}^{(qN)}$ in our calculations.

In Appendix A a brief description of the derivation of the di-quark exchange contact potential is given. This is based on a phenomenological description of the confinement-deconfinement at high nucleon-densities via a nucleon-triquark λ_3-coupling, using a quark-diquark description of the triquark. The resulting NJL-type quark-nucleon interaction is

$$\mathcal{L}_{int}^{(2)} \;=\; -\lambda_3^2 \left(\bar{\psi}(x)\gamma_5\gamma_\mu \boldsymbol{\tau} Q\right) \cdot \left(\bar{Q}\gamma_5\gamma^\mu \boldsymbol{\tau}\psi\right) / \mathcal{M}^2 \tag{2.2}$$

with $\mathcal{M} = \hbar c$. (Choosing $\mathcal{M}$ differently merely means a rescaling of λ_3.) In (2.2) we used the isospin spinor $Q = (u, d)$.

The di-quark exchange (central) potential from the Lagrangian (2.2) is given by [50]

$$\begin{aligned} V_{DQE}^{(qN)}(r) = &-\lambda_3^2 \frac{\Lambda}{4\pi\sqrt{\pi}} \frac{\Lambda^2}{\mathcal{M}^2} \, (\boldsymbol{\tau}_1 \cdot \boldsymbol{\tau}_2)(\boldsymbol{\sigma}_1 \cdot \boldsymbol{\sigma}_2) \, \mathcal{P}_x \cdot \\ &\times \left[1 - \frac{3\Lambda^2}{4 m_N m_q} \left(1 - \frac{\Lambda^2 r^2}{6}\right)\right] \exp\left[-\frac{\Lambda^2 r^2}{4}\right], \end{aligned} \tag{2.3}$$

where the baryon-triquark coupling λ_3 in MeV^{-2}, $\mathcal{P}_x$ the space-exchange operator, and Λ and $\mathcal{M}$, can be treated as adjustable parameters.

Considering the chiral symmetry breaking as the QCD non-perturbative effect, constituent quark masses in quark matter become smaller than those in vacuum and move to current masses in the

high-density limit. In our previous works [21, 22], we introduced phenomenologically the density-dependent quark mass

$$M_Q^*(\rho_Q) = M_0/[1 + \exp\{\gamma(\rho_Q - \rho_c\}] + m_0 + C \tag{2.4}$$

with $C = M_0 - M_0/[1 + \exp(-\gamma\rho_c)]$ assuring $M_Q^*(0) = M_0 + m_0$, where ρ_Q is quark density. The effect of using this quark masses is demonstrated in Fig.11, where the parameters are chosen as $\rho_c = 7\rho_0$, $M_0 = 362$ MeV and $\gamma = 1.2$ [22].

C. Framework of Nucleon-Quark mixed matter

Our nucleon-quark mixed matter is composed of nucleons (n and p^+), quarks (u and d) and electrons (e^-), where a nucleon number density ρ_N is given by a sum of neutron and proton densities, $\rho_N = \rho_n + \rho_p$, and a quark number density ρ_q by a sum of u-quark and d-quark densities, $\rho_q = \rho_u + \rho_d$. In our treatment of nucleon-quark mixed matter, the BHF framework is adopted on the basis of two-body NN, qq and qN potentials. Correlations induced by bare potentials are renormalized into coordinate-space G-matrix interactions, treated as effective two-body interactions used in matter calculations. G-matrix interactions $\mathcal{G}_{NN'}$, $\mathcal{G}_{qN}$, $\mathcal{G}_{qN}$ and $\mathcal{G}_{qq'}$ with $N, N' = n, p$ and $q, q' = u, d$ are derived from the above bare NN, qN and qq interactions. They are given for each (T, S, P) state, T, S and P being isospin, spin and parity in a two-body state, respectively.

Single particle potentials of N and q are given by

$$\begin{aligned} U_N(k) &= \sum_{N'=n,p} U_N^{(N')}(k) + \sum_{q'=u,d} U_N^{(q')}(k) \\ &= \sum_{N'=n,p} \sum_{k'<k_F^{(N')}} \langle kk'|\mathcal{G}_{NN'}|kk'\rangle \\ &\quad + \sum_{q'=u,d} \sum_{k'<k_F^{(q')}} \langle kk'|\mathcal{G}_{Nq'}|kk'\rangle \end{aligned} \tag{2.5}$$

$$\begin{aligned} U_q(k) &= \sum_{q'=u,d} U_q^{(q')}(k) + \sum_{N'=n,p} U_q^{(N')}(k) \\ &= \sum_{q'=u,d} \sum_{k'<k_F^{q'}} \langle kk'|\mathcal{G}_{qq'}|kk'\rangle \\ &\quad + \sum_{N'=n,p} \sum_{k'<k_F^{(N')}} \langle kk'|\mathcal{G}_{qN'}|kk'\rangle \end{aligned} \tag{2.6}$$

where k_F^N and k_F^q is the Fermi momenta of nucleon N and quark q, respectively. Spin and isospin quantum numbers are implicit.

The quark energy density for $q = u, d$ in our nucleon-quark mixed matter is given by

$$\begin{aligned} \varepsilon_q &= m_q\rho_q + g_s N_c \int_0^{k_F^q} \frac{d^3k}{(2\pi)^3} \\ &\quad \left\{ \sqrt{\hbar^2k^2 + m_q^2} + \frac{1}{2}U_q(k) \right\} . \end{aligned} \tag{2.7}$$

where Fermion spin and quark-color degeneracies give rise to $g_s = 2$ and $N_c = 3$, respectively.

The nucleon energy density for $N = n, p$ is given by

$$\begin{aligned}\varepsilon_N &= m_N\rho_N + \tau_N + \upsilon_N \\ &= m_N\rho_N + g_s\int_{k_0^N}^{k_1^N}\frac{d^3k}{(2\pi)^3} \\ &\quad\left\{\sqrt{\hbar^2k^2+m_N^2}+\frac{1}{2}U_N(k)\right\}\ . \end{aligned} \tag{2.8}$$

It is necessary, here, to explain upper and lower limits of integral (k_0^N and k_1^N). In the simple case of deriving NQMM-A EoSs, they are chosen as $k_1^N = k_F^N$ and $k_0^N = 0$ as usual.

On the other hand, in the case of deriving NQMM-B EoSs, according to the concept of the quarkyonic matter [41], where interacting quarks near the Fermi sea form interacting neutrons, and the remaining quarks fill the lowest momenta up to k_F^q. The nucleon Fermi levels of $0 < k < k_F^N$ are pushed up to those of $k_0^N < k < k_1^N$ as a result that nucleons below k_0^N are excluded by the Pauli principle.

Then, k_0^N and k_1^N are given as follows: The density of the nucleon Fermi sphere with radius k_0^N is given by $\frac{(k_0^N)^3}{3\pi^2}$, and the density of the quark Fermi sphere with radius k_F^q is given by $\rho_q = \frac{3N_c(k_F^q)^3}{3\pi^2}$. Considering that the k_0^N value is determined by the condition that the densities of nucleon and quark Fermi spheres are equal to each other, we have

$$\frac{(k_0^N)^3}{3\pi^2} = \rho_q\ , \tag{2.9}$$

from which the value of k_0^N is obtained. The value of k_1^N is obtained from the relation

$$\frac{(k_1^N)^3}{3\pi^2} - \frac{(k_0^N)^3}{3\pi^2} = \frac{(k_F^N)^3}{3\pi^2} = \rho_N\ . \tag{2.10}$$

These values of k_0^N and k_1^N are lower and upper limits of the integral in Eq.(2.8). The relations (2.9) and (2.10) are considered as plausible assumptions to determine k_0^N and k_1^N, respectively, which plays a decisive role to give nucleon partial pressures pushed up by the quark Fermi repulsion in the NQMM-B case. In this work, it is out of our scope to derive the quark Fermi repulsion more microscopically.

Here, the potential-energy part in Eq.(2.8) is approximated by the following expression

$$\bar{\upsilon}_N = g_s\int_0^{k_F^N}\frac{d^3k}{(2\pi)^3}\left\{\frac{1}{2}U_N(k)\right\}\ , \tag{2.11}$$

meaning that the Fermi repulsion for low-momentum neutrons are determined by kinetic-energy densities. Furthermore, this Fermi exclusion effects for low-momentum components are neglected for protons.

Our total energy density is given by

$$\varepsilon = \varepsilon_n + \varepsilon_p + \varepsilon_u + \varepsilon_d + \varepsilon_e\ . \tag{2.12}$$

The chemical potential μ_i ($i = n, p, u, d, e$) and pressure P are expressed as

$$\mu_i = \frac{\partial \varepsilon_i}{\partial \rho_i} , \tag{2.13}$$

$$P = \sum_{i=n,p,u,d,e} \mu_i \rho_i - \varepsilon . \tag{2.14}$$

When P and ε are given, sound velocities are defined by $c_s^2 = \partial P / \partial \varepsilon$. Our BHF framework is basically non-relativistic, and a causal condition of $c_s < c$ is not always assured: In regions of $c_s > c$, sound velocities are approximated to be $c_s = c$.

In the EoS of β-stable nucleon-quark mixed matter composed of n, p, u, d and e, the equilibrium conditions are given as

(1) chemical equilibrium conditions,

$$\mu_n = \mu_p + \mu_e \tag{2.15}$$

$$\mu_n = \mu_u + 2\mu_d \tag{2.16}$$

(2) charge neutrality,

$$\rho_p = \rho_e \tag{2.17}$$

(3) baryon number conservation,

$$\rho = \rho_n + \rho_p + \rho_Q , \tag{2.18}$$

where ρ_Q is a baryonic (3 quarks) number density which is related to a quark number density ρ_q by $\rho_Q = \rho_q/3$ with $\rho_q = \rho_u + \rho_d$, and ρ is a total number density. For simplicity, the ratio of u and d quarks in nucleon-quark mixed matter is assumed to be $\rho_u/\rho_d = 1/2$ as well as the one in neutron-quark mixed matter, and the equilibrium condition $\mu_p = 2\mu_u + \mu_d$ is not taken into account.

Defining $Y_p = \rho_p/\rho_N$ with $\rho_N = \rho_n + \rho_p$ and $Y_Q = \rho_Q/(\rho_N + \rho_Q)$, energy densities ($\varepsilon_n$, ε_p, ε_u, ε_d) and chemical potentials (μ_n, μ_p, μ_u, μ_d) are given as a function of ρ_N, Y_p and Y_Q. Then, Y_p and Y_Q values included in the EoS are obtained by solving the equations $\mu_n = \mu_p + \mu_e$ (2.15) and $\mu_n = \mu_u + 2\mu_d$ (2.16). Solutions are obtained in an approximate way: First, Y_p values are obtained by solving the equation $\mu_n = \mu_p + \mu_e$ for given values of ρ_N within nucleon components (taking $Y_Q = 0$) in nucleon-quark mixed matter. Next, Y_Q values are obtained by solving the equation $\mu_n = \mu_u + 2\mu_d$ for given values of ρ_N and Y_p. The radius of the quark Fermi sphere (Fermi momentum) k_F^q is related to Y_Q by

$$k_F^q = (3\pi^2 Y_Q(\rho_N + \rho_Q))^{1/3} . \tag{2.19}$$

Then, lower and upper limits of the integral in Eq.(2.8), k_0^N and k_1^N, are obtained by using (2.9) and (2.10), meaning that the Y_Q values determine the nucleon Fermi layer pushed up by the Fermi repulsion.

The quark-mixing rates Y_Q are determined by the equilibrium condition Eq.(2.16) for nucleon and quark chemical potentials. The latter includes constituent quark masses m_q, values of which

are related sensitively to onset densities of quark mixing in nucleonic matter. A simple choice of constituent quark mass is $m_q = m_N/3 = 313$ MeV. In [55], however, they obtain $m_q = 362$ MeV which is determined to reproduce $m_N = 938$ MeV with the confining and one-gluon exchange potentials among three quarks. We adopt their values of 362 MeV for constituent quark masses. It is confirmed that this large value of 362 MeV is favorable to give larger values of quark onset densities than the small value of 313 MeV, being important for deriving reasonable MR curves of neutron stars. For further tuning of quark onset densities, we introduce corrections for mass terms of quark chemical potentials by replacing m_q to $m_q + \Delta m_q$ with parameters Δm_q. This tuning of quark onset densities by m_q is important for obtaining reasonable MR curves.

In the above, our quark states in nucleon-quark mixed matter are represented in the BHF framework, where formations of e.g. superconducting pairs are neglected, which could probably soften the EoS. In the confinement-deconfinement mechanism considered in this paper the naturally appearing diquarks have spin-1. This means that in the ground-state of matter they do not condensate because of rotational invariance, unless one assumes e.g. a strong spin-spin attraction between pairs causing (quasi) spin-less bound states. An extension to include color superconducting spin-zero diquarks with use of the Hartree-Fock-Bogoliubov (HFB) theory and the impact on the softening of the EoS is an interesting future problem.

III. RESULTS AND DISCUSSION

The EoSs are derived from NQMM-A and NQMM-B for nucleon-quark mixed matter, respectively, without and with the Pauli-exclusion effect for neutrons from the quark Fermi sphere. The adjustable parameters included in these EoSs are (1) the nucleon-triquark coupling constant $\lambda 3$ in $V_{DQE}^{(QN)}$ and (2) the corrections Δm_q for constituent quark masses:
(1) Nucleon-triquark coupling constants are chosen as $\lambda_3/\sqrt{4\pi}$= 0, 0.1, 0.2, 0.4, 0.8, 1.5, and resulting qN interactions are denoted as $\lambda 0$, $\lambda 01$, $\lambda 02$, $\lambda 04$, $\lambda 08$, $\lambda 15$, respectively. Here $\lambda_3/\sqrt{4\pi}$=0 ($\lambda 0$) means to take only the meson-exchange parts $V_{EME}^{(QN)}$ without the direct-quark-exchange parts $V_{DQE}^{(QN)}$. The limiting case of switching off all qN and qq interactions is denoted as "qt", where only kinetic energies are taken into account in free quark states. In Fig.11, the density-dependent quark mass Eq.(2.4) is used in the $\lambda 15$ case, denoted as $\lambda 15'$.
(2) Parameters Δm_q control onset densities for quark mixing: In the cases of NQMM-A (NQMM-B), parameters Δm_q are chosen so that the onset density is $2.5\rho_0$, $2.0\rho_0$ and $1.6\rho_0$ with ρ_0=0.17fm^{-3}, which are denoted as NQMM A16, NQMM A20 and NQMM A25 (NQMM B16, NQMM B20 and NQMM B25), respectively. For instance, a NQMM-A EoS for $\lambda 15$ with an onset density $2.0\rho_0$ is denoted as NQMM A20-$\lambda 15$.

For each qN interaction, values of Δm_q are determined so as to give onset densities $2.5\rho_0$, $2.0\rho_0$ and $1.6\rho_0$. The determined values of Δm_q are tabulated in Table I.

TABLE I: Values of Δm_q (MeV).

	qt	$\lambda 0$	$\lambda 01$	$\lambda 02$	$\lambda 04$	$\lambda 08$	$\lambda 15$
$2.5\rho_0$	15.	10.	25.	40.	65.	120.	200.
$2.0\rho_0$	−5.	−15.	−5.	10.	30.	70.	140.
$1.6\rho_0$	−20.	−28.	−20.	−10.	5.	40.	90.

A. EoS

Let us demonstrate the repulsive qN interactions. In Fig.1, averaged potential energy of neutron $\langle U_n \rangle$ in the case of $Y_p = 0$ are drawn as a function of neutron number density ρ_n. $\langle U_n \rangle$ is defined by the expression

$$\langle U_n \rangle = \sum_{q=u,d} \frac{1}{\rho_q} \int_0^{k_F^q} \frac{d^3k}{(2\pi)^3} U_n^{(q)}(k) \tag{3.1}$$

where $U_n^{(q)}(k)$ given by Eq.(2.5) are obtained from qn interactions. Dotted, short-dashed and solid curves are obtained in the cases of qn interactions $\lambda 0$, $\lambda 04$ and $\lambda 15$, respectively, where thick (thin) curves are in the cases of $Y_Q = 0.2$ (0.6). It is noted that the repulsive contributions of $\langle U_n \rangle$ by qn repulsions increase rapidly with density ρ_n, which work to stiffen EoSs in high density regions. Even in the case of $\lambda 0$, there exists the weakly repulsive contribution from $V_{EME}^{(QN)}$.

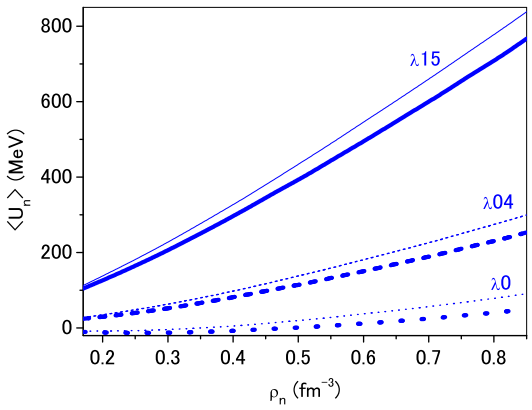

FIG. 1: (Color online) Averaged potential energy of neutron $\langle U_n \rangle$ given by Eq.(2.5) as a function of neutron number density ρ_n. Dotted, short-dashed and solid curves are obtained in the cases of $\lambda 0$, $\lambda 04$ and $\lambda 15$, respectively, Thick (thin) curves are in the cases of $Y_Q = 0.2$ (0.6).

In our nucleon-quark mixed matter, the quark mixing rate Y_Q is determined by the chemical equilibrium condition $\mu_n = \mu_u + 2\mu_d$ Eq.(2.16) with chemical potentials μ_n, μ_u and μ_d. In Fig.2, values of Y_Q are given as a function of total density $\rho = \rho_N + \rho_Q$. The solid, short-dashed, dotted and thin-solid curves are in the cases of $\lambda 15$, $\lambda 04$, $\lambda 0$ and qt, respectively, in the case of onset

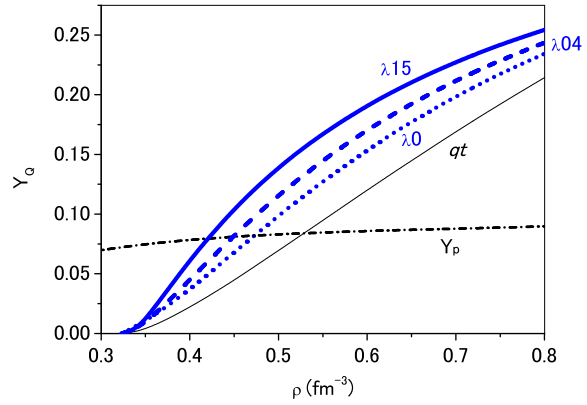

FIG. 2: (Color online) Quark mixing rates Y_Q given as a function of total density $\rho = \rho_N + \rho_Q$. Solid, short-dashed, dotted and thin-solid curves are in the cases of $\lambda 15$, $\lambda 04$, $\lambda 0$ and qt, respectively, in the case of onset density $2.0\rho_0$. Dot-dashed curve is proton mixing rates Y_P as a function of ρ.

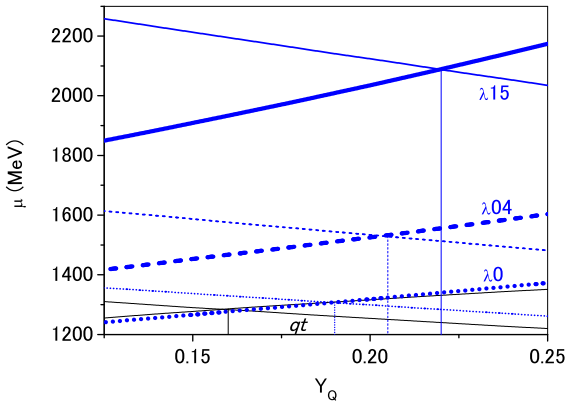

FIG. 3: (Color online) Neutron (quark) chemical potentials μ_n ($\mu_u + 2\mu_d$) as a function of Y_Q in the case of $\rho = \rho_N + \rho_Q = 4\rho_0$. Solid, short-dashed, dotted and thin-solid curves are in the cases of $\lambda 15$, $\lambda 04$, $\lambda 0$ and qt, respectively, in the case of onset density $2.0\rho_0$. Increasing and decreasing curves show $\mu_u + 2\mu_d$ and μ_n, respectively. Y_Q values satisfying equilibrium conditions ($\mu_n = \mu_u + 2\mu_d$) are given by abscissa values of cross points, where Y_Q values for $\lambda 15$, $\lambda 04$, $\lambda 0$ and qt are 0.22, 0.205, 0.19 and 0.16, respectively.

density $2.0\rho_0$. In the important density region lower than about $5\rho_0$, the Y_Q values are noted to become larger, as the qN interactions become more repulsive from $\lambda 0$ to $\lambda 15$. For reference, the Y_p values as a function of ρ are shown by the dot-dashed curve.

The relations between the Y_Q values and the strengths of qN repulsions are demonstrated in Fig.3, where the quark and neutron chemical potentials $\mu_u + 2\mu_d$ and μ_n are drawn as a function of Y_Q in the case of total density $\rho = \rho_N + \rho_Q = 4\rho_0$. The solid, short-dashed, dotted and thin-solid curves are in the cases of $\lambda 15$, $\lambda 04$, $\lambda 0$ and qt, respectively, in the case of onset density $2.0\rho_0$.

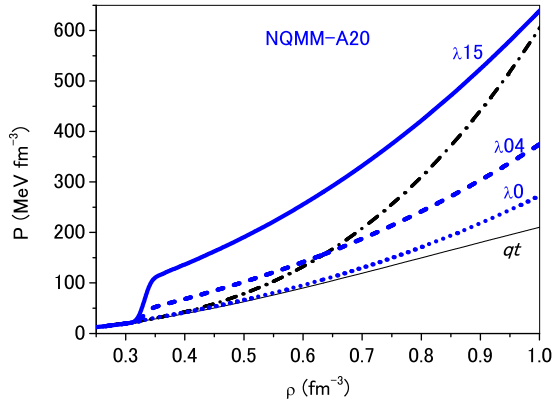

FIG. 4: (Color online) Partial pressures of nucleons as a function of total density $\rho = \rho_N + \rho_Q$. The dot-dashed curve is pressures in nucleonic matter. Solid, short-dashed, dotted and thin-solid curves are pressures for $\lambda 15$, $\lambda 04$, $\lambda 0$ and qt, respectively, in the case of NQMM-A20.

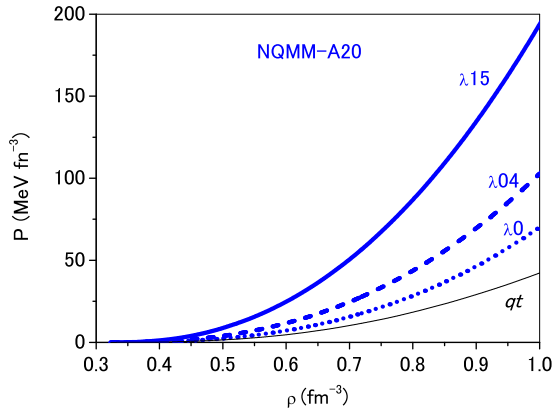

FIG. 5: (Color online) Partial pressures of free quarks as a function of total density $\rho = \rho_N + \rho_Q$. Sold, short-dashed, dotted and thin-solid curves are pressures for $\lambda 15$, $\lambda 04$, $\lambda 0$ and qt, respectively, in the case of NQMM-A20.

The increasing (decreasing) curves show $\mu_u + 2\mu_d$ (μ_n), and the chemical equilibrium conditions $\mu_n = \mu_u + 2\mu_d$ are satisfied at cross points of increasing and decreasing curves, namely Y_Q values satisfying equilibrium conditions are given by abscissa values of cross points, as indicated by vertical lines. The Y_Q values at cross points are noted to become larger as the qN interactions become more repulsive, which is the reason why the Y_Q values in Fig.2 become larger as the qN interactions become more repulsive.

In Fig.4 and Fig.5, partial pressures of nucleons and free quarks, P_N and P_Q, are given as a function of total density $\rho = \rho_N + \rho_Q$, respectively. In Fig.4, the dot-dashed curve is pressures in nucleonic matter. The solid, short-dashed, dotted and thin-solid curves are pressures for $\lambda 15$,

$\lambda 04$, $\lambda 0$ and qt, respectively, in the case of NQMM-A20. In Fig.5, solid, short-dashed, dotted and thin-solid curves are pressures P_Q of free quarks for $\lambda 15$, $\lambda 04$, $\lambda 0$ and qt, respectively, in the case of NQMM-A20. P_Q values increase when the qN repulsions and Y_Q values increase from $\lambda 0$ to $\lambda 15$. Anyway, partial pressures of free quarks are substantially smaller than those of neutrons.

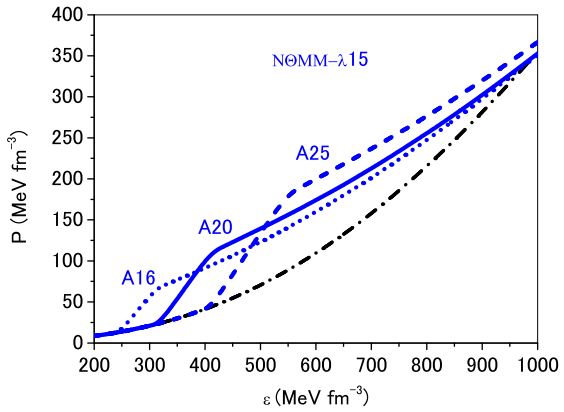

FIG. 6: (Color online) Pressures as a function of energy densities for NQMM-$\lambda 15$. Solid, short-dashed and dotted curves are in the cases of A20, A25 and A16. The dot-dashed curve is pressures in nucleonic matter.

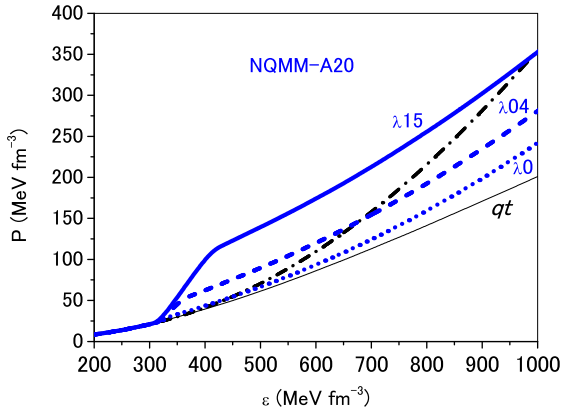

FIG. 7: (Color online) Pressures as a function of energy densities for NQMM-A20. Solid, short-dashed, dotted and thin-solid curves are in the cases of $\lambda 15$, $\lambda 04$, $\lambda 0$ and qt, respectively. The dot-dashed curve is pressures in nucleonic matter.

In Fig.6, pressures P for NQMM-A EoSs are drawn as a function of the energy density ε, that is $P(\varepsilon)$, in the cases of $\lambda 15$ with different quark onset densities. The solid, short-dashed and dotted curves are in the cases of A20, A25 and A16, respectively. The dot-dashed curve is pressures in nucleonic matter. The branching points of the above three curves from this dot-dashed curve are related to the quark onset densities. Sudden increase in pressure at a quark onset point means that

the derivative $\partial P/\partial\varepsilon$ is discontinuous, and the phase transition from nucleonic matter to nucleon-quark mixed matter is second-order. As shown later, such a rapid change of pressure for energy density produces a peak in the speed of sound [20].

In Fig.7, pressures P for NQMM-A20 EoSs are drawn as a function of the energy density ε in the case of quark onset density $2.0\rho_0$. The dot-dashed curve is pressures in nucleonic matter. The solid, short-dashed, dotted and thin-solid curves are in the cases of $\lambda 15$, $\lambda 04$, $\lambda 0$ and qt, respectively. The solid curve in this figure is the same as the solid one in Fig.6, both of which are obtained by NQMM A20-$\lambda 15$. One should note, here, the remarkable reduction of pressures from the dot-dashed curve for nucleonic matter to the thin-solid curve (qt), which can be considered as the EoS softening caused by quark mixing in the case of no qN and qq repulsions. In the cases of $\lambda 15$ and $\lambda 04$ with strong qN di-quark repulsions, the EoS softening is recovered by sudden increases in pressure at quark onset points. In the case of $\lambda 0$, such effects are not so noticeable.

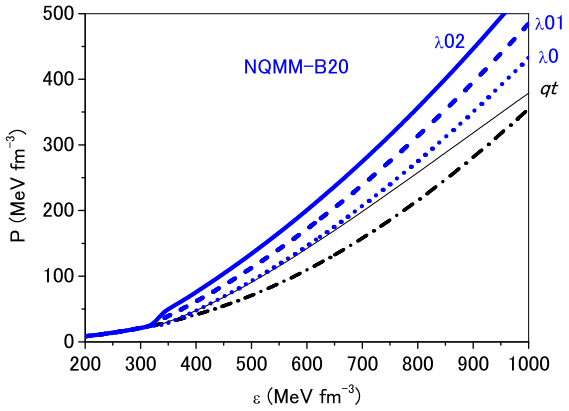

FIG. 8: (Color online) Pressures as a function of energy densities for NQMM-B20 EoSs. Solid, short-dashed, dotted and thin-solid curves are in the cases of $\lambda 15$, $\lambda 04$, $\lambda 0$ and qt, respectively. The dot-dashed curve is pressures in nucleonic matter.

In Fig.8, pressures P are drawn as a function of the energy density ε for NQMM-B20 EoSs with quark onset density $2.0\rho_0$. The dot-dashed curve is pressures in nucleonic matter. The solid, short-dashed, dotted and thin-solid curves are obtained in the cases of $\lambda 15$, $\lambda 04$, $\lambda 0$ and qt, respectively. These curves are noted to be above the dot-dashed curve for nucleonic matter. The curves for $\lambda 15$ and $\lambda 04$ are pushed up by the combined effects of the Fermi repulsions for nucleons from the quark Fermi sphere and the di-quark exchange qN repulsions.

In Fig.9, pressures P for NQMM-$\lambda 02$ EoSs are drawn as a function of the energy density ε for different quark onset densities. The solid, short-dashed and dotted curves are in the cases of B20, B25 and B16, respectively. The solid curve in this figure is the same as the solid one in Fig.8, both of which are obtained for NQMM B20-$\lambda 02$. The dot-dashed curve is pressures in nucleonic matter. The different quark onset densities lead to the different branching points from the dot-dashed curve. Sudden increase in pressure at a quark onset point (second-order phase transition) is related to rising of a MR curve at a corresponding onset density, producing a peak in the speed of sound.

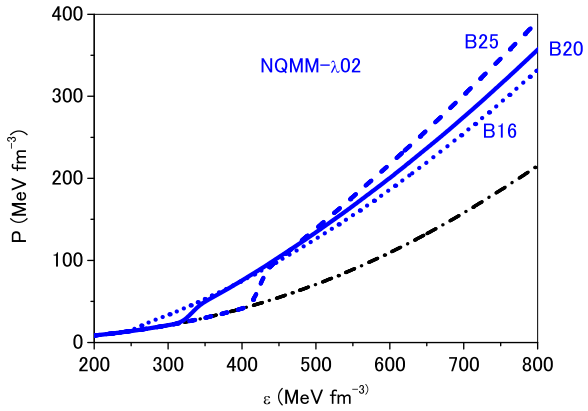

FIG. 9: (Color online) Pressures as a function of energy densities for NQMM-λ02. Solid, short-dashed and dotted curves are in the cases of B20, B25 and B16. The dot-dashed curve is pressures in nucleonic matter.

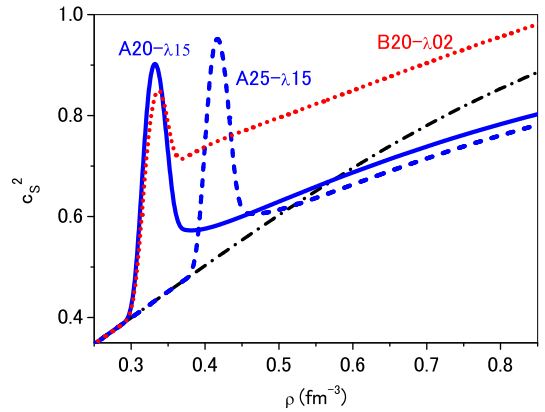

FIG. 10: (Color online) Sound velocities $c_s^2 = \partial P/\partial\varepsilon$ are drawn as a function of baryonic density $\rho = \rho_N + \rho_Q$. The dot-dashed curve is sound velocities in the nucleonic matter. Solid, short-dashed and dotted curves are sound velocities in nucleon-quark mixed matter for NQMM A20-λ15, A25-λ15 and B20-λ02, respectively.

In Fig.10, sound velocities $c_s^2 = \partial P/\partial\varepsilon$ in nucleon-quark mixed matter are drawn as a function of total density $\rho = \rho_N + \rho_Q$. The dot-dashed curve is sound velocities in the nucleonic matter. Solid, short-dashed and dotted curves are sound velocities in the cases of NQMM A20-λ15, A25-λ15 and B20-λ02, respectively, where the peaks appear at quark onset densities $2.0\rho_0$ (A20 and B20) and $2.5\rho_0$ (A25). The peak structures of sound velocities are produced by the second-order phase transitions from nucleonic to nucleon-quark mixed states at quark onset densities. This mechanism is the same as the one in [41].

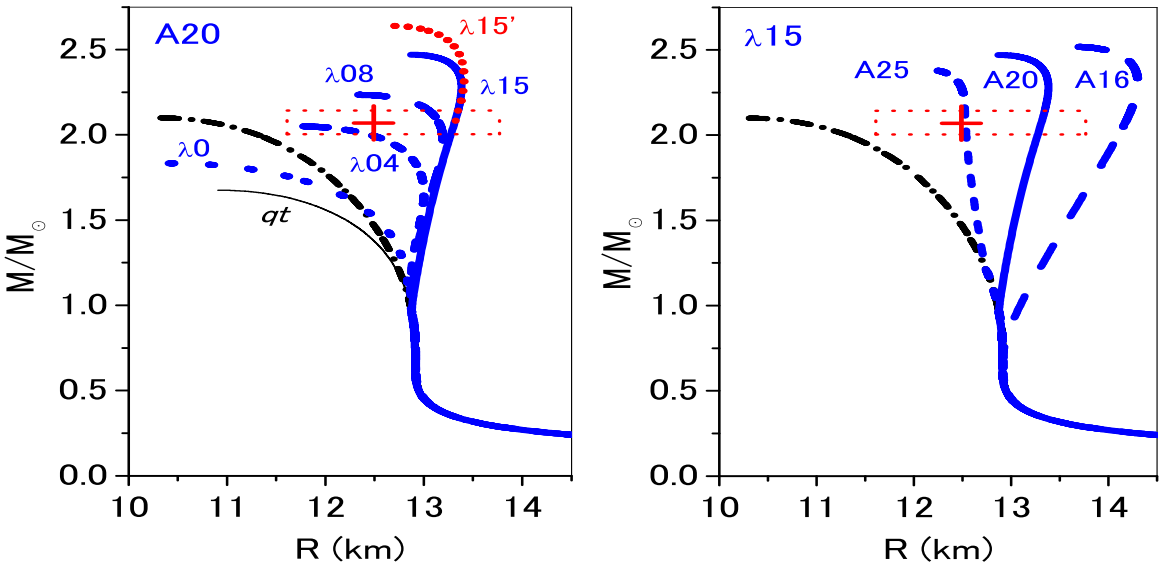

FIG. 11: (Color online) Star masses as a function of radius R for NQMM-A EoSs. In the left panel, thin-solid, dotted, short-dashed, dashed, solid and short-dotted curves are for qt, $\lambda 0$, $\lambda 04$, $\lambda 08$, $\lambda 15$ and $\lambda 15'$, respectively, in the cases of the onset density $2.0\rho_0$ (A20). In the right panel, $M(R)$ curves are for $\lambda 15$ with different quark onset densities. Solid, short-dashed and dashed curves are in the cases of onset densities $2.5\rho_0$ (A25), $2.0\rho_0$ (A20) and $1.6\rho_0$ (A16), respectively. In both panels, the dot-dashed curves are for the nucleonic matter EoS.

B. MR diagrams

We have the EoSs for several models of nucleon-quark mixed matter (MQMM-A and NQMM-B). These EoSs are connected to the crust EoS [56, 57] at $\rho = 0.22$ fm^{-3} with smooth interpolations. Star masses M as a function of radius R, that is $M(R)$, are obtained by solving the TOV equations with these EoSs for nucleon-quark mixed matter.

In the following figures for $M(R)$ curves, the regions given by $M = 2.08 \pm 0.07 M_\odot$ and $R = 12.49^{+1.28}_{-0.88}$ km [26] are drawn by dotted rectangles, and the point ($M = 2.1 M_\odot$, $R_{2.1M_\odot}$=12.5 km) is indicated by a cross symbol. In the analysis of $M(R)$ curves, our critical guideline is that an obtained $M(R)$ curve reaches above this cross symbol in the MR diagram.

In the right panel of Fig.11, star masses are given as a function of radius R for the NQMM-A EoSs in the cases of $\lambda 15$ with different quark onset densities, corresponding to the $P(\varepsilon)$ curves in Fig.6. The dot-dashed curves are obtained by the nucleonic matter EoS. The solid, short-dashed and dashed curves are in the cases of quark onset densities $2.0\rho_0$ (A20), $2.5\rho_0$ (A25) and $1.6\rho_0$ (A16), respectively.

In the left panel of Fig.11, star masses are given as a function of radius R for NQMM-A EoSs in the case of quark onset density $2.0\rho_0$. The thin-solid, dotted, short-dashed, dashed and solid curves are in the cases of qt, $\lambda 0$, $\lambda 04$, $\lambda 08$ and $\lambda 15$, respectively. The dot-dashed curve is obtained by the nucleonic matter EoS. The thin-solid curve (qt) is obtained by the EoS in which all qN

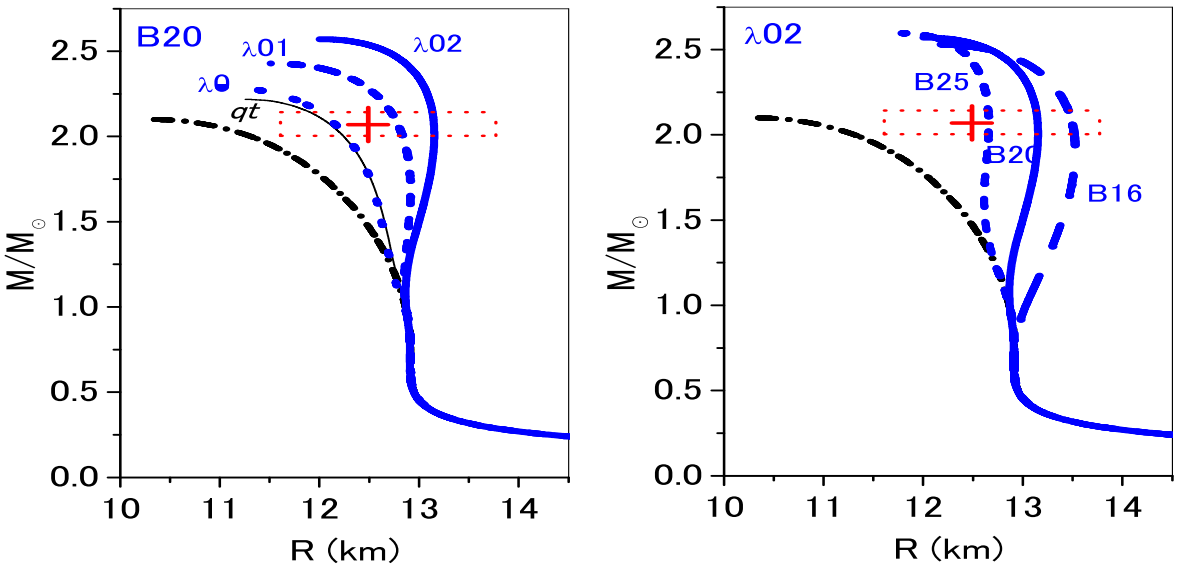

FIG. 12: (Color online) Star masses as a function of radius R for NQMM-B EoSs In the left panel, the thin-solid, dotted, short-dashed and solid curves are for qt, $\lambda 0$, $\lambda 01$ and $\lambda 02$, respectively. In the right panel, $M(R)$ curves are for $\lambda 02$ with different quark onset densities. Solid, short-dashed and dashed curves are in the cases of onset densities $2.5\rho_0$ (B25), $2.0\rho_0$ (B20) and $1.6\rho_0$ (B16), respectively. In both panels, the dot-dashed curves are obtained by the nucleonic matter EoS.

and qq interaction are switched of. The reason of the small maximum mass in this case is because of the EoS softening caused by changing of high-momentum neutrons at Fermi surfaces to low-momentum free quarks, which is the same as the mechanism of the EoS softening by hyperon mixing. It should be noted that the $M(R)$ curves are pushed up by the increasing qN repulsions from $\lambda 0$ to $\lambda 15$. The short-dotted curve above the solid curve for $\lambda 15$ is obtained by using the density-dependent quark mass Eq.(2.4) in the case of $\lambda_3/\sqrt{4\pi}$=1.5 (denoted as $\lambda 15'$) and the quark onset density $2.0\rho_0$. The $M(R)$ curve turns out to be pushed up further by the density-dependent effects of quark masses.

In Fig.12, star masses are given as a function of radius R for NQMM-B EoSs. In the left panel, the thin-solid, dotted, short-dashed and solid curves are obtained for qt, $\lambda 0$, $\lambda 01$ and $\lambda 02$, respectively, with quark onset density $2.0\rho_0$. In the right panel, they are obtained for $\lambda 02$ EoSs with different quark onset densities. The solid, short-dashed and dashed curves are in the cases of quark onset densities $2.0\rho_0$ (B20), $2.5\rho_0$ (B25) and $1.6\rho_0$ (B16), respectively. The dot-dashed curves in both panels are obtained by the nucleonic matter EoS. The $M(R)$ curves (onset density $2.0\rho_0$) in the left panel are of good correspondence to the $P(\varepsilon)$ curves in Fig.8. It should be noted that all $M(R)$ curves for nucleon-quark mixed matter EoSs are above this dot-dashed curve differently from those in the left panel of Fig.11. Though the $M(R)$ curve for NQMM-A (qt) gives small maximum mass due to the EoS softening, the curve for NQMM-B (qt) is pushed up by the Fermi repulsion for nucleons from the quark Fermi sphere and give maximum mass over that for the nucleonic EoS.

In Fig.12, the $M(R)$ curves for $\lambda 01$ and $\lambda 02$ are pushed up by the combined effects of the quark Fermi repulsions and the increasing qN di-quark exchange repulsions.

In Fig.13, star masses are given as a function of central baryon density ρ_{Bc}, that is $M(\rho_{Bc})$. The dot-dashed curve is obtained by the nucleonic EoS. The solid, short-dashed and dotted curves are by NQMM A20-λ15, A25-λ15 and B20-λ02, respectively. The behaviors of $M(\rho_{Bc})$ curves respond well to the corresponding $P(\varepsilon)$ curves in Fig.7 and Fig.8. The $P(\varepsilon)$ curves, as well as the $M(\rho_{Bc})$ curves, are noted to be above the dot-dashed curves by the nucleonic EoS.

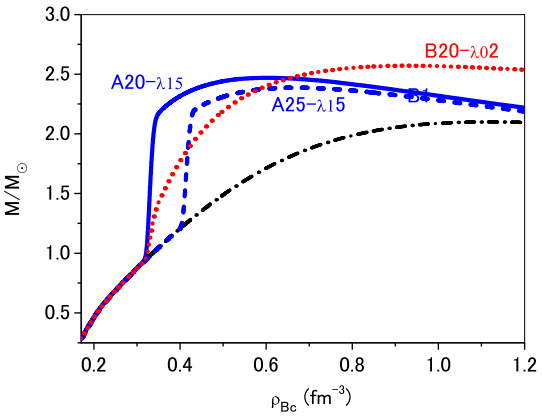

FIG. 13: (Color online) Star masses as a function of central baryon density ρ_{Bc}. The dot-dashed curve is obtained by the nucleonic EoS. Solid, short-dashed and dotted curves are by NQMM A20-λ15, A25-λ15 and B20-λ02, respectively.

Table II summarize the values of maximum masses $M_{max}/M_{\odot}$ and radii $R_{2.1M_{\odot}}$ (km) found in Fig.11 and Fig.12, where the values of $R_{2.1M_{\odot}}$ turn out to be consistent with the observed data $R = 12.49^{+1.28}_{-0.88}$ km [26].

IV. CONCLUSION

The nucleon-quark mixed matter is defined in the BHF framework, which is suitable to treat qN and qq interactions without being obscured by ad hoc parameters such as thickness Δ of neutron Fermi layer used in the quarkyonic matter [41]. In this framework the quark density in nucleon-quark mixed matter is determined by the equilibrium conditions between chemical potentials of nucleons and free quarks. Our qN interaction is composed of meson-exchange and di-quark exchange potentials, playing critical roles for our nucleon-quark mixed matter EoS. The di-quark potential is strongly repulsive and the nucleon-triquark coupling constant plays a role as a critical parameter for the stiffness of our EoS. In the nucleon-quark mixed matter, Fermi spheres of nucleons and free quarks are occupied by nucleons with momenta of $0 < k < k_F^N$ and quarks with momenta of $0 < k < k_F^q$, respectively, from which NQMM-A EoSs are derived straightforwardly. Taking the basic concept of quakyonic matter [41] into account, the nucleon Fermi levels are pushed up to the one with momenta of $k_0^N < k < k_1^N$ (Fermi layer) by the Fermi exclusion effect

TABLE II: Values of maximum masses $M_{max}/M_\odot$ and radii $R_{2.1M_\odot}$ (km) at $2.1M_\odot$ obtained for NQMM-A and NQMM-B EoSs. NUC give the values for nucleonic matter EoS.

		$M_{max}/M_\odot$	$R_{2.1M_\odot}$ (km)
A20	qt	1.68	
	$\lambda 0$	1.83	
	$\lambda 4$	2.05	
	$\lambda 8$	2.23	13.1
	$\lambda 15$	2.47	13.3
	$\lambda 15'$	2.64	13.3
A25	$\lambda 15$	2.37	12.5
B20	qt	2.22	12.0
	$\lambda 0$	2.23	12.1
	$\lambda 1$	2.43	12.8
	$\lambda 2$	2.57	13.1
B25	$\lambda 2$	2.60	12.7
NUC		2.10	11.3

for nucleons from the quark Fermi sphere. The NQMM-B EoSs are derived by incorporating this quark Fermi repulsion into our nucleon-quark mixed matter.

Our EoSs are controlled basically by the strength of di-quark exchange repulsion and the effective quark mass: The former and latter determine the stiffness of EoS and the quark onset density, respectively. Then, the phase transition from nucleonic matter to nucleon-quark mixed matter is second-order, and there appear peak structures in sound velocities at quark onset densities.

The features of our nucleon-quark mixed matter are demonstrated by pressures as a function of energy density $P(\varepsilon)$ and neutron-star mass-radius curves $M(R)$. In the cases of NQMM-A EoSs, the $P(\varepsilon)$ and $M(R)$ curves for nucleon-quark mixed matter are pushed up above those for nucleonic matter by the qN repulsive interactions, as found in Fig.7 and Fig.11. These pushing-up effects are further enhanced by taking account of density dependences of quark masses. In the limiting case of switching off all qN and qq interactions, the $M(R)$ curves are far below the curves for nucleonic matter, which can be considered as remarkable EoS softening caused by changing of high-momentum neutrons to low-momentum free quarks. As qN repulsions increase, the MR curves for nucleon-quark mixed matter are pushed above the point ($M = 2.1M_\odot$, $R_{2.1M_\odot}$=12.5 km) indicated by the recent radius observation of the massive neutron stars. In our nucleon-quark mixed matter different from the quakyonic matter [41], these pushing-up effects for MR curves are realized by the strong qN repulsions in NQMM-A EoSs, without taking account of the Fermi exclusion effect for nucleons from the quark Fermi sphere included in NQMM-B EoSs.

In the cases of NQMM-B EoSs, the $P(\varepsilon)$ and $M(R)$ curves for nucleon-quark mixed matter are always above those for nucleonic matter, as found in Fig.8 and Fig.12, respectively. Even if the qN repulsions are switched off, the MR curves come near the point ($M = 2.1M_\odot$, $R_{2.1M_\odot}$=12.5 km) owing to the Fermi repulsion for nucleons from the quark Fermi sphere. In the case of NQMM-B EoSs, the pushing-up effects for MR curves are realized by additive contributions from the qN

repulsions and the Fermi exclusion effect from the quark Fermi sphere.

Our approach to neutron-star EoSs is based on the nucleon-quark mixed matter in the BHF framework, in which the qN di-quark exchange repulsions play important roles. The derived EoSs are consistent with observed data of M_{max} and $R_{2M_\odot}$. In relation to the "hyperon puzzle", there still remains the issue of the size of an EoS softening induced by hyperon/s-quark mixing in the nucleon/baryon-quark mixed matter. The extension to include hyperons and strange-quarks is a natural step in the further development of this work. Furthermore, an extension by incorporating color superconductivity spin-zero pairs using the HFB theory, studying e.g. the impact on the softening of the EoS is interesting.

Acknowledgments

The author (N.Y.) was supported by JSPS KAKENHI Grant Number 24K07054.

Appendix A: Di-quark exchange Interaction

The di-quark exchange potential $V_{DQE}^{(qN)}$ is derived from a description of the confinement-deconfinement process at high baryon-densities via the (density dependent) nucleon-triquark coupling

$$\mathcal{L}_{int}^{(1)} = -\lambda_3 \left[\bar{\psi}(x)\eta_N(x) + \bar{\eta}_N(x)\psi(x)\right] \tag{A1}$$

with [51]

$$\eta_N(x) = \left[\widetilde{q}^a(x) C\gamma^\mu q^b(x)\right] \gamma_5\gamma_\mu q^c(x) f^{abc}, \tag{A2}$$

where C is the charge conjugation operator, and momentarily we left out the isospin labels.
The interaction Lagrangian in (A1) with the tri-quark field $\eta_N(x)$ is rewritten using di-quark fields for two reasons: (i) the functional form of the partition function is difficult to handle, and (ii) di-quarks are meaningful physical entities. In terms of the (bosonic) di-quark fields $\chi_\mu^a(x)$

$$\eta_N(x) \;=\; (\hbar c)^2 \gamma_5\gamma^\mu q^a(x) \cdot \chi_\mu^a(x), \tag{A3a}$$

$$\chi_\mu^a(x) \;\equiv\; f^{abc}\widetilde{q}^b(x) C\gamma_\mu q^c(x)/(\hbar c)^2. \tag{A3b}$$

The interaction (A1) becomes

$$\mathcal{L}_{int}^{(1)} = -\lambda_3(\hbar c)^2 \left[\left(\bar{\psi}(x)\gamma_5\gamma^\mu q^a(x)\right) \chi_\mu^a(x) + h.c.\right] \tag{A4}$$

Using the grand-canonical partition functional $\mathcal{Z}_G$ description of matter and treating $\chi_\mu^a(x)$ within the auxiliary field method [52] by introducing the $\chi_\mu^a(x)$-field via the Lagrangian

$$\mathcal{L}_\chi = \bar{\lambda}_3^2 \left\{ \chi_\mu^{a\dagger}(x)\chi^{\mu a}(x) - \left[\chi_\mu^{a\dagger}(x)\left(\tilde{q}^b(x) C\gamma^\mu q^c(x)\right) f^{abc} + h.c.\right] \right\} \tag{A5}$$

the partition functional becomes, see [53],

$$Z_G = \int [d\bar{\psi}][d\psi][d\bar{q}][dq][d\sigma][d\omega_\mu] \int \mathcal{D}\chi^{a\mu}\mathcal{D}\chi_\mu^{a\dagger} \exp\Bigg[\int_0^\beta d\tau \int d^3x \cdot$$
$$\times\big(\mathcal{L}_N + \mathcal{L}_Q + \mathcal{L}_M + \mathcal{L}_\chi + \mu_N\psi^\dagger\psi + \mu_Q q^\dagger q\big)\Bigg]. \tag{A6}$$

For example in the Walecka-model [54]

$$\mathcal{L}_Q \rightarrow \bar{q}(x)\left[i\gamma_\mu\left(\partial^\mu + \frac{i}{3}g_\omega\omega^\mu\right) - \left(m_Q - \frac{1}{3}g_\sigma\sigma\right)\right] q(x) \tag{A7a}$$

$$\mathcal{L}_N \rightarrow \bar{\psi}(x)\left[i\gamma_\mu\left(\partial^\mu + ig_\omega\omega^\mu\right) - \left(m_N - g_\sigma\sigma\right)\right] \psi(x) \tag{A7b}$$

$$\mathcal{L}_M \rightarrow +\frac{1}{2}\left(\partial^\mu\sigma\partial_\mu\sigma - m_\sigma^2\sigma^2\right) - \frac{1}{4}\omega_{\mu\nu}\omega^{\mu\nu} + \frac{1}{2}m_\omega^2\omega_\mu\omega^\mu \tag{A7c}$$

The terms in $\mathcal{L}_\chi$ are schematically, apart from an overall factor $\bar{\lambda}_3^2$,

$$\mathcal{L}_\chi \sim \quad \chi_\mu^\dagger\chi^\mu - \chi_\mu^\dagger B^\mu - B_\mu^\dagger\chi^\mu = (\chi_\mu - B_\mu)^\dagger(\chi^\mu - B^\mu) - B_\mu^\dagger B^\mu, \tag{A8}$$

with $B_\mu = \left[\bar{\psi}(x)\gamma_5\gamma_\mu q(x)\right]/(\hbar c)^2$. The integration over the shifted $\left(\chi_\mu^a - B_\mu^a\right)$ di-quark fields gives in the exponential of Z_G the term

$$-\bar{\lambda}_3^2\, B_\mu^\dagger B^\mu = -\bar{\lambda}_3^2(\bar{\psi}\gamma_5\gamma_\mu q)(\bar{q}\gamma_5\gamma^\mu\psi) \tag{A9}$$

where $\bar{\lambda}_3 \equiv \lambda_3/(\hbar c)$. The Lagrangian in $\mathcal{Z}_G$ becomes $\mathcal{L} = \mathcal{L}_N + \mathcal{L}_Q + \mathcal{L}_M + \mathcal{L}_{int}^{(2)}$ with

$$\mathcal{L}_{int}^{(2)} = -\bar{\lambda}_3^2\, B_\mu^\dagger B^\mu = -\bar{\lambda}_3^2\left(\bar{\psi}\gamma_5\gamma_\mu q\right)\left(\bar{q}\gamma_5\gamma^\mu\psi\right), \tag{A10}$$

which is the interaction in (2.2).

---

[1] P.B. Demorest, T. Pennucci, S.M. Ransom, M.S.E. Roberts, and J.W. Hessels, Nature (London) **467**, 1081 (2010).

[2] J. Antoniadis *et al.*, Science **340**, 6131 (2013).

[3] H.T. Cromartie *et al.*, Nat. Astron. **4**, 72 (2020).

[4] R.W. Romani *et al.*, Astrophysical J. Lett. **934**, L17 (2022).

[5] A. Drago, A. Lavagno, G. Pagliara, and D. Pigato, Phys. Rev. C **90**, 065809 (2014).

[6] D.B. Kaplan, A.E. Nelson, Phys. Lett. B **175**, 57 (1986); **179**, 409 (1986).

[7] G.E. Brown, C.-H. Lee, M. Rho, and V. Thorsson, Nucl. Phys. A **567**, 937 (1994).

[8] V. Thorsson, M. Prakash, and J.M. Lattimer, Nucl. Phys. A **572**, 693 (1994).

[9] C.-H. Lee, Phys. Rep. **275**, 255 (1996).

[10] N.K. Glendenning and J. Schaffner-Bielich, Phys. Rev. Lett. **81**, 4564 (1998).

[11] M.Baldo, G.F. Burgio, and H-J. Schulze, *Superdense QCD Matter and Compact stars (NATO Science Series 2: Mathematics, Physics and Chemistry vol. 197)* (2006) ed D.Blaschke and D. Sedrakian.

[12] F. Özel, D. Psaltis, S. Ransom, P. Demorest, and M. Alford, Astrophys. J. Lett. **724**, L199 (2010).
[13] I. Sagert, G. Pagliara, M, Hempel, and Schaffner-Bielich, Astrophys. J. Lett. **740**, L14 (2011).
[14] T. Kähn, D. Blaschke, and D. Lastowiecki, Phys. Rev. D **88**, 085001 (2013).
[15] L. Bonanno and A. Sedrakian, Astrophys. J. **539**, 416 (2012).
[16] R. Lastowiecki, D. Blaschke, H. Grigorian, and S. Typel, Acta Phys. Pol. **B5**, 535 (2012).
[17] M. Shahrbaf, D. Blaschke, A.G. Grunfeld, and H.R. Moshfegh, Phys. Rev. C **101**, 025807 (2020).
[18] M. Shahrbaf, D. Blaschke, and S. Khanmohamadi, J. Phys. G: Nucl. Part. Phys. **47**, 115201 (2020).
[19] K. Otto, M. Oertel, and B-J Schaefer, Phys. Rev. D **101**, 103021 (2020); arXiv:1910.11929 (2020)
[20] T. Kojo, G. Baym, and T. Hatsuda, Astrophys. J. **934**, 46 (2022), arXiv:2111.11919 (2022).
[21] Y. Yamamoto, N. Yasutake, and Th. A. Rijken, Phys. Rev. C **105**, 015804 (2022).
[22] Y. Yamamoto, N. Yasutake, and Th. A. Rijken, Phys. Rev. C **108**, 035811 (2023).
[23] M.C. Miller *et al.*, Astrophys. J. Lett. **918**, L28 (2021), arXiv:2105.06979 [astro-ph.HE]
[24] T.E. Riley *et al.*, Astrophys. J. Lett. **918**, L27 (2021), arXiv:2105.06980 [astro-ph.HE]
[25] I. Legred, K. Chatziioannou, R. Essick, S. Han, and P. Landy, Phys. Rev. D **104**, 063003 (2021),
[26] T. Salmi *et al.*, arXiv:2406.14466 [astro-ph.HE]
[27] A.J. Dittmann *et al.*, arXiv:2406.14467 [astro-ph.HE]
[28] S. Nishizaki, Y. Yamamoto, and T. Takatsuka, Prog. Theor. Phys. **105**, 607 (2001); **108**, 703 (2002).
[29] I. Vidaña,D. Logoteta, C. Providência, A. Polls, and I. Bombaci, Eur. Phys. Lett. **94**, 1002 (2011).
[30] Y. Yamamoto, T. Furumoto. Yasutake, and Th.A Rijken, Phys. Rev. C **90**, 045805 (2014).
[31] Y. Yamamoto, T. Furumoto, N. Yasutake, and Th.A Rijken, Eur. Phys. J. A **52**, 19 (2016).
[32] Y. Yamamoto, H. Togashi, T. Tamagawa. T. Furumoto, N. Yasutake, and Th.A. Rijken, Phys. Rev. C **96**, 065804 (2017).
[33] D. Lonardoni A. Lovato, S. Gandolfi, and F. Pederiva, Phys. Rev. Lett. **114**, 092301 (2015).
[34] D. Logoteta, I. Vidaña, I. Bombaci, Eur. Phys. J. A **55**, 207 (2019).
[35] D. Cerstung, N. Kaiser. and W. Weise, Eur. Phys. J. A **56**, 175 (2020).
[36] M. M. Nagels, Th. A. Rijken, and Y. Yamamoto, Phys. Rev. C **99**, 044002 (2019).
[37] M. M. Nagels, Th. A. Rijken, and Y. Yamamoto, Phys. Rev. C **99**, 044003 (2019).
[38] M. M. Nagels, Th. A. Rijken, and Y. Yamamoto, Phys. Rev. C **102**, 054003 (2020).
[39] L. McLerran and H.D. Pisarski, Nucl. Phys. A **796**, 83 (2007).
[40] Y. Hidaka, L. McLerran, and H.D. Pisarski, Nucl. Phys. A **808**, 117 (2008).
[41] L. McLerran and S. Reddy, Phys. Rev. Lett. **122**, 122701 (2019).
[42] S. Han, M.A.A. Mamun, S. Lalit, C. Constantinou, and M. Prakash, Phys. Rev. D **100**, 103022 (2019).
[43] D.C. Duarte, S. Hernande-Ortiz, and K.S. Jeong, Phps. Rev. C **102**, 025203 (2020); 065202 (2020).
[44] T. Zhao and J.M. Lattimer, Phys. Rev. D **102**, 023021 (2020).
[45] J. Margueron, H. Hansen, and P. Proust, and G.Chanfray, Phys. Rev. C **104**, 055803 (2021).
[46] G. Cao Phys. Rev. D **105**, 114020 (2022).
[47] A. Akmal, V.R. Pandharipande, and D.G. Ravenhall, Phys. Rev. C **58**, 1804 (1998).
[48] H. Togashi and M. Takano, Nucl. Phys. A **902**, 53 (2013).
[49] Th.A. Rijken and Y. Yamamoto, *Quark-Quark and Quark-Nucleon potential Model. ESC Meson-exchange Interactions*, Report THEF-NIJM 24.02, unpublished, `https://nn-online.org/eprints` (2024).
[50] Th.A. Rijken, *Quark-Nucleon Di-quark-exchange Potentials*, Report THEF-NIJM 24.03, unpublished, `https://nn-online.org/eprints` (2024).
[51] B.L. Ioffe, Nucl. Phys, B **188**, 317 (1981); B.L. Ioffe and A.V. Smilga, Nucl. Phys. B **232**, 109 (1984).
[52] C.M. Bender and F. Cooper, Ann. of Phys. (N.Y.) **109**, 165 (1977).
[53] J.I. Kapusta and C. Gale, *Finite-Temperature Field Theory. Principles and Applications*, Cambridge

University Press, Cambridge, England (1989), Chapter 11.
[54] J.D. Walecka, Ann. of Phys. (N.Y.) **83**, 491 (1974).
[55] N. Yasutake and T. Maruyama, Phys. Rev. D **109**, 043056 (2024).
[56] G. Baym, A. Bethe, and C. Pethick, Nucl. Phys. A **175**, 225 (1971).
[57] G. Baym, C.J. Pethick, and P. Sutherland, Astrophys. J. **170**, 299 (1971).